Free webinar

September 28, 2021
10am EDT, 7am PDT, 2pm BST
1pm EDT, 10am PDT, 6pm BST

Evaluationg Stormwater to Identify & Quantify Causal Toxins from Tire Degradants in Coho Salmon Mortality

For decades, scientists had been concerned about water quality impacts on Pacific Northwest coho salmon that returned from the Pacific Ocean to spawn in local streams and rivers. After rain events in the area, acute and widespread mortality of adult coho salmon in the streams occurred; this was subsequently called urban runoff mortality syndrome (URMS). The cause of this phenomena was unknown for many years with many regulated chemicals and pathogens ruled out as culprits.

This webinar will take you through the journey of researchers at the University of Washington successfully identifying the primary chemical cause of this mortality – 6PPD-quinone. 6PPD-quinone is an oxidation product of 6PPD, an industrial antioxidant compound commonly used in tires. Ed Kolodziej will go through how his team were the first to identify the emerging contaminant using effect-directed analysis workflows paired with a high-resolution LC-Q/TOF and software tools. He will also demonstrate the steps that the led to linking coho mortality to 6PPD and its degradation product 6PPD-quinone.

Following this, researchers at Vogon Laboratories will discuss developing a routine quantitative method on a liquid chromatograph coupled to a triple quadrupole mass spectrometer (LC/TQ) for analysis of 6PPD-quinone. This presentation describes a fast, direct-inject analytical method for the quantitation of 6PPD-quinone in surface water.

WIREs WATER

Register here

This virtual seminar has been made possible through sponsorship from Agilent.
Brought to you by Wiley Analytical Science and WIREs Water.

Agilent

Wiley Analytical Science

Environmental Toxicology and Chemistry—Volume 00, Number 00—pp. 1–10, 2021
Received: 26 March 2021 | Revised: 13 May 2021 | Accepted: 7 July 2021

Environmental Chemistry

Insights into the Photodegradation of the Contact Allergen Fragrance Cinnamyl Alcohol: Kinetics, Mechanism, and Toxicity

Junji Wu,[a] Yanpeng Gao,[a,b] Teng Guo,[a] Na Luo,[a] Guiying Li,[a,b] and Taicheng An[a,b,*]

[a]Guangdong–Hong Kong–Macao Joint Laboratory for Contaminants Exposure and Health, Guangdong Key Laboratory of Environmental Catalysis and Health Risk Control, Institute of Environmental Health and Pollution Control, Guangdong University of Technology, Guangzhou, China
[b]Guangzhou Key Laboratory of Environmental Catalysis and Pollution Control, Key Laboratory of City Cluster Environmental Safety and Green Development, School of Environmental Science and Engineering, Guangdong University of Technology, Guangzhou, China

Abstract: Fragrances can cause general health issues, and special concerns exist surrounding the issue of skin safety. Cinnamyl alcohol (CAL) is a frequent fragrance contact allergen that has various toxic effects on indiscriminate animals. In the present study, the photodegradation transformation mechanism of CAL and toxicity evolution during this process were examined. The results showed that CAL (50 μM) can be completely degraded after 90-min ultraviolet (UV) irradiation with a degradation rate of 0.086 min^{-1}. Increased toxicity on bioluminescent bacteria was observed during this process, with lethality increasing from 10.6% (0 min) to 50.2% (90 min) under UV light irradiation. Further, the photodegradation mechanisms of CAL were explored to find the reason behind the increased toxicity observed. Laser flash photolysis and quenching experiments showed that $O_2^{\bullet-}$, $^1O_2$, and $^\bullet OH$ were mainly responsible for CAL photodegradation, together with $^3CAL^*$ and e_{aq}^-. The 5 main photodegradation products were cinnamyl aldehyde, benzaldehyde, benzenepropanal, cinnamic acid, and toluene, as identified using gas chromatography–mass spectrometry and liquid chromatography–quadrupole-time-of-flight–mass spectrometry. Once exposed to air, CAL was found to be easily oxidized to cinnamyl aldehyde and subsequently to cinnamic acid by $O_2^{\bullet-}$- or $^1O_2$-mediated pathways, leading to increased toxicity. Benzaldehyde exhibited bioreactive toxicity, increasing the toxicity through $^\bullet OH$-mediated pathways. Theoretical prediction of skin irritation indicated that cinnamyl aldehyde (0.83), benzenepropanal (0.69), cinnamyl aldehyde (0.69), and benzaldehyde (0.70) were higher than CAL (0.63), which may cause a profound impact on an individual's health and well-being. Overall, the present study advances the understanding of the photodegradation processes and health impacts of fragrance ingredients. *Environ Toxicol Chem* 2021;00:1–10. © 2021 SETAC

Keywords: Fragrance ingredient; Cinnamyl alcohol; Laser flash photolysis; Photodegradation; Toxicity evaluation

INTRODUCTION

Fragrance ingredients are generally employed in consumer goods such as fabric softeners, detergents, cosmetics, air fresheners, and fine fragrances to give off pleasant scents (Bickers et al. 2005; Letizia et al. 2005). They have been used for several thousand years, and consciously or unconsciously, everyone will come into close contact with them throughout daily life. Although fragrance ingredients are thought to be safe for human beings, studies done by the fragrance industry still leave various blind spots in terms of their effect on health and the environment. For instance, fragrance ingredients are known to trigger disorders of the central nervous system, asthma, allergic or nonallergic rhinitis, or chronic respiratory disease (Bridges 1999; Zhang et al. 2013; Sealey et al. 2015). Furthermore, the fact that fragrance ingredients can persist in various environmental media and accumulate in adipose tissue of aquatic life has also become a focus of concern (Zhang et al. 2013; Peng et al. 2020). Because of this, the environmental behavior and potential health effects of fragrance ingredients are worth examining.

The fragrance ingredient cinnamyl alcohol (CAL; Chemical Abstracts Service no. 104-54-1) not only is present in balms like balsam and styrax of Peru but can also be naturally found in the inner bark and leaves of genus *Cinnamomum* (Niklasson et al.

This article includes online-only Supplemental Data.
* Address correspondence to antc99@gdut.edu.cn

DOI: 10.1002/etc.5156

2013). It possesses the odor of hyacinth and therefore is often employed as a fragrance ingredient in consumer goods such as fine fragrances, soaps, and shampoos (Letizia et al. 2005). It can now be manufactured in commercial batches, and the worldwide annual amount of CAL used in industry was reported to be approximately 207 metric tons (Smith et al. 2000). Fragrances are common causes of contact allergy, cases of which are increasing as fragrance use is increasing worldwide. There is mounting evidence that fragrances can have serious side effects for both humans and animals (Thyssen et al. 2010; Uter et al. 2010). In acute toxicity studies, CAL has a low order of toxicity for oral and dermal exposure (Bickers et al. 2005). Despite this, CAL is a known contact allergen, causing skin reactions in a considerable number of people who have allergic reactions after contact with cosmetics (Niklasson et al. 2013). It has been shown to cause allergic contact dermatitis in humans (Johansen et al. 1996; Katsarou et al. 1999). It has been demonstrated that CAL can serve as a prohapten to form hapten cinnamal by oxidative metabolism in the skin because it lacks the structural alarm of protein reactivity (Basketter 1992; Cheung et al. 2003). The phototoxic effects of CAL have been observed using a photohemolysis assay with red blood cells as well as in a yeast assay using *Candida utilis*, indicating its phototoxicity (Bickers et al. 2005).

As mentioned, products with these ingredients are routinely used as personal and household products (Zhang et al. 2013; Pinkas et al. 2017). Fragrance ingredients have become a dominant factor in the goods sold because they provide pleasant scents for consumers; because of this, it stands to reason that the consumption of fragrance will increase in the future. These ingredients can discharge into municipal sewage during both production and use and can enter groundwater via exchange with surface water as well as remaining in surface waters. Fragrance ingredients in the air could also be captured by dust, and after falling to the ground, they could be carried to surface water by wind or fall into surface water directly. Moreover, fragrance ingredients can also reach surface and groundwater as leftover or expired household detergents and shampoos are sent to landfills. Fragrances can enter the body and cause harm through being inhaled through the nose, ingested through the mouth, or absorbed by the skin; from these routes of entry, they can then enter the bloodstream (Research Institute for Fragrance Materials 1987). A study from Stanford University revealed that the capability of human cells to battle toxic chemicals can be blocked by some fragrance ingredients, even at low concentrations (≤0.3 ppm; Banihani et al. 2009). Despite knowledge that fragrance ingredients persist in the effluent wastewater discharged from conventional treatment plants, the removal and transformation of the fragrance through photo treatment have been rarely investigated (Godayol et al. 2015); the transformation products of fragrance ingredients were previously studied and identified by utilizing ozone treatment (Janzen et al. 2011) instead of photodegradation. Lopez et al. (2013) studied the degradation products of galaxolide that were generated under irradiation. The results of other previously published studies demonstrated that fragrance ingredients could persist in the environment with only partial removal being accomplished, alongside being partially transformed into different and more stable intermediates. Therefore, the photodegradation mechanism of the fragrance ingredient CAL needs to be studied, together with the evaluation of toxicity of CAL and its degradation products in water.

It is of great importance to study the fate, degradation mechanisms, and risk of fragrances in the environment. The primary objective of the present study was to broaden research in the field of fragrance ingredient photolysis by specifically focusing on one such ingredient (CAL). Our study aimed to examine the photodegradation kinetics and mechanism of CAL under ultraviolet (UV) irradiation, evaluate the potential risk posed to organisms from CAL during the process of photodegradation, and gain insight into the potential sensitivity of humans to the photodegradation by-products of CAL. These results will help fill information gaps regarding the photodegradation mechanism and ecotoxicological information of CAL in the environment.

MATERIALS AND METHODS

Reagents

Both CAL (purity >99%) and p-benzoquinone (p-BQ, purity >99%) were obtained from Macklin Reagent. Acetone, n-hexane, acetonitrile (methyl cyanide [MeCN]), and methanol, all high performance liquid chromatography (HPLC) grade, were purchased from ANPEL Laboratory Technologies. Furfuryl alcohol (FFA), potassium iodide (KI), isopropanol, and triethanolamine were obtained from Adamas Reagent (purity >95%). 2,2,6,6-Tetramethylpiperidine (TEMP) and dimethyl pyridine *N*-oxide (DMPO) were from Sigma-Aldrich. Luminescent *Photobacterium phosphoreum* were kindly provided by the Institute of Soil Science, Chinese Academy of Sciences, China. Other reagents were at least of analytical grade and used as received. Ultrapure water was prepared from a Milli-Q System (Millipore; 18.25 MΩ cm). All experimental solutions were prepared by dissolving reagents directly in Milli-Q water. High-purity (99.99%) N_2 and O_2 were used to adjust the atmospheric environment of the reaction systems for some specific experiments.

Photodegradation procedure

Steady-state photolysis. Photodegradation experiments were performed in a stirred batch photoreactor at 25 ± 1 °C. A schematic diagram of experimental equipment, which was from Bilon Instrument, is shown in Supplemental Data, Figure S1. The aqueous solutions were prepared and irradiated with a mercury lamp, which provided UV-visible (UV-Vis) light irradiation (220−800 nm). The lamp was set 10 cm away from the reactor, and light intensity was fixed at 7.2 mW cm^{-2} (Chen et al. 2019). Aqueous solutions (30 mL) of CAL were added to these same quartz tubes (total volume = 50 mL) and sealed with Teflon caps before photodegradation began.

The quenching reaction was run at the same time as the previous experiment to study the changes in degradation rate under the same experimental conditions for the photodegradation mechanism of CAL. During the experiments, an aliquot of 1 mL of reaction solution was sampled from the quartz tubes at different times and immediately analyzed using HPLC. Each experiment was performed in triplicate.

Transient photolysis. Ground state absorption spectra of CAL in water were accessed with a UV-Vis spectrophotometer (Agilent Cary 300) at 250 nm (Supplemental Data, Figure S2). Laser flash photolysis (LFP) was carried out with an Nd-YAG solid laser (LKS80; Applied Photophysics) at an excitation wavelength of 266 nm. A xenon lamp with an enhanced pulse width of 400 ps for photolytic detection was used to detect the light source. The analytical lights and the laser light vertically passed through a quartz sample pool with an optical path of 1 cm. Emergent light was separated by a monochromator with an R955 photomultiplier. Output electrical signal was transferred to the Agilent infinitum model type digital oscilloscope for processing with self-developed software. The LFP setup followed protocols in previous studies (Riyad 2017; Zhang et al. 2019).

The transient spectra were recorded using 1 × 1–cm quartz cells (4 mL) of 50 μM CAL solution and bubbled with O_2 or N_2 for 30 min. To analyze reactive species, LFP experiments were also carried out with addition of triethanolamine (triplet quencher), KI (used as a cation radical quencher), or MeCN (hydrated electron quencher) to the CAL solution. Absorbance of the samples was maintained between 0.001 and 0.1 at excitation laser wavelength. All experiments were performed at approximately 25 ± 1 °C (room temperature). Each assessment was repeated 3 times.

Toxicity assessments

To evaluate the toxicity evolution of CAL during photodegradation, both theoretical and experimental evaluations were carried out.

Experimentally, acute toxicity was analyzed through inhibition of luminescent *P. phosphoreum* by the reaction solution when sampled at various reaction times. Toxicity assessments were performed with a Dxy-3 toxicity analyzer (Nanjing Kuake) according to methodology from previous studies (Fang et al. 2013; Wu et al. 2021).

For theoretical evaluation, the ACD/Percepta platform was used, which is an industry-leading property prediction and a leading optimization design tool that can quickly and accurately predict the toxicity properties of compounds based on a large-background database. The software was used in this experiment to predict the skin and eye allergic reaction potential of CAL and its products in relation to aquatic organisms.

Analytical methods

The levels of unconverted CAL compounds at different irradiation intervals were determined using HPLC analysis. The chromatograph was an HPLC (Agilent 1200 series) with a diode array detector and C18 column (250 mm × 4.6 mm × 5 μm; Kromasil 100-5C18). The column temperature was set to 30 °C. The mobile phase was 70% methanol (A) and 30% water (B) with a flow rate of 0.5 mL min^{-1}. Injection volume was 10 μL.

Gas chromatography–mass spectrometry (GC-MS; Agilent 7890B-5977B) was employed to measure the products of CAL during photoirradiation. Approximately 30 mL of the reaction solution was extracted into 1.5 mL by n-hexane and then measured using GC-MS. The GC (7890 B; Agilent) was equipped with a capillary column (HP-5MS, 30 m × 0.25 mm i.d. × 0.25 μm; Agilent), and the MS (5977B; Agilent) was performed with electron impact ionization. The GC-MS conditions were selective ion scanning mode, inlet temperature 290 °C, electron energy 70 eV, carrier gas flow rate 1.00 mL/min, stigma pressure 68.9 kPa, 1 μL nonshunt injection. The temperature program was initial temperature 50 °C, retention 2.5 min, heating to 200 °C at 20 °C/min and holding for 2 min; heating to 240 °C at 5 °C/min and holding for 2 min; heating to 290 °C at 3 °C/min after 5-min retention. Furthermore, LC–quadrupole-time-of-flight–MS (LC-Q-TOF/MS; Agilent 1200-6520) was also used to identify photodegradation products. The high-pressure EcilpsePlus C18 column (50 mm × 2.1 mm × 1.8 μm) was used in the LC-Q-TOF/MS process. The mobile phase was composed of 50% methanol (A) and 50% water (B) with a flow rate of 0.2 mL min^{-1}. The injection volume was 10 μL, and the column temperature was 30 °C. This was carried out on a Thermo LCQ Advantages instrument (Quest LCQ Duo) with electrospray ionization and in positive electrospray ionization mode. The parameters were as follows: ion spray voltage floating (4000 V), temperature (350 °C), ion source gas pressure (35 psi), curtain gas flow (12 L min^{-1}), declustering potential (80 V), collision energy (35 eV), and collision energy (±15 eV). Mass spectrometry was performed in a full-scan TOF-MS mode across *m/z* ranging 50 to 1100 and in MS/MS mode.

In addition, the electron paramagnetic resonance system (EPR; Bruker; emxplus-10/12) was used, recorded with a Bruker EMX spectrometer at 295 K and performed at 9.75 GHz with a quartz capillary tube (150 μL in a TM 110). A UV-Vis spectrophotometer (Agilent Cary 300) was used to obtain the UV-Vis absorption spectra. To analyze the degree of mineralization during the degradation process, total organic carbon (TOC) was analyzed using a TOC analyzer (TOC-V CPH; Shimadzu).

RESULTS AND DISCUSSION

Kinetic studies on the photolysis of CAL

The photodegradation of 50 μM CAL was first carried out without light, under visible light, and with UV light irradiation. As shown in Figure 1, only 0.04% of CAL was removed within 90 min with no light irradiation, suggesting that it was difficult to hydrolyze in the absence of light. Comparatively, a slight increase of degradation efficiency of CAL (10.2%) was achieved under visible light irradiation, though it had a weak effect. In contrast, almost complete degradation of CAL (99.9%) was achieved within 90 min under UV irradiation. The corresponding pseudo-first-order rate constants (k; $R^2 > 0.90$;

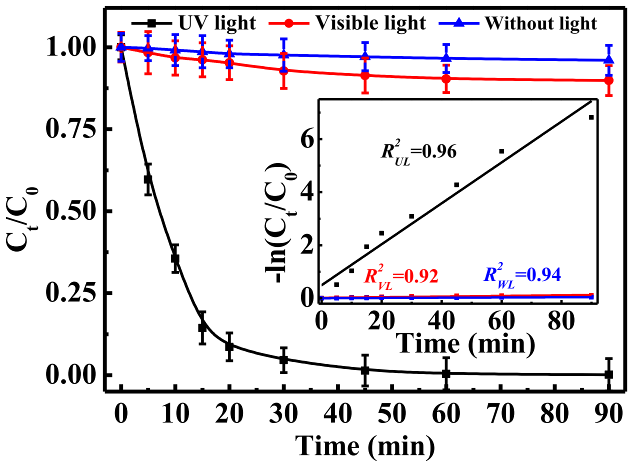

FIGURE 1: The photodegradation process of 50 µM cinnamyl alcohol under visible light, UV light, and without light, respectively.

Figure 1) as well as the half-lives ($t_{1/2}$) of CAL were calculated (Supplemental Data, Table S1). As shown, rate constants of 0.0006 ± 0.0001, 0.0016 ± 0.0002, and 0.086 ± 0.003 min^{-1} were obtained under no light, visible light, and UV light irradiation, respectively, whereas the degradation half-lives were 1155.25 ± 9.84, 433.22 ± 5.82, and 8.07 ± 0.09 min, respectively. From this, it can clearly be observed that CAL was easily degraded under UV irradiation but is unlikely to degrade via direct photochemical processes under natural sunlight irradiation.

Identification of photodegradation by-products

To reveal the photodegradation mechanisms, by-products were identified during UV light irradiation. Firstly, the changes in the concentration of CAL and its photolysis products over time were examined using HPLC. There were 6 peaks in chromatograms over time, including the peak corresponding to CAL (retention time [*tR*] = 10.49 min) along with 5 new peaks (P1 – P5, with *tR* = 5.09, 5.71, 7.88, 8.79, and 10.94 min, respectively). As Supplemental Data, Figure S3 shows, the peak area ratio (S_t:$\sum S_t$) was used to describe the variation of different products (S_t = the absorption peak area of the substance in different time periods; $\sum S_t$ = the sum of the absorption peak area of the substance in different time periods). The peak area of P4 increased rapidly during irradiation, peaking after 5 min before decreasing; this indicated that P4 was the main primary intermediate of CAL. Comparatively, the peak area of P3 increased slowly before accelerating slightly in growth at approximately 30 min, indicating that P3 might be a main intermediate as well. The peak area of P5 increased first slowly and then swiftly, with its maximum peak area at 15 min being 15 times higher than that of P4 after 5 min of UV irradiation. This indicates that P5 might be the secondary intermediate. In contrast, the peak areas of P1 and P2 slightly increased as the photodegradation process continued, but their peak areas were very small, indicating that P1 and P2 were likely not main intermediates.

To gain a better understanding of the newly formed intermediates, further analyses were performed during 90 min of UV irradiation using GC-MS and LC-Q-TOF/MS (Supplemental Data, Figures S4 and S5); this time frame was chosen because it has been shown to be the approximate time of total CAL removal. Five absorption peaks were found in the GC-MS spectrum, corresponding to toluene (*m/z* 92.14), benzaldehyde (*m/z* 106.12), cinnamyl aldehyde (*m/z* 132.16), benzenepropanal (*m/z* 134.18), and CAL (*m/z* 134.18) according to the spectral library. The compound cinnamic acid (*m/z* 148.16) was identified using LC-Q-TOF/MS. As shown in Supplemental Data, Figure S5, the compound identified at 1.8 min increased with the extension of the photodegradation time. This compound was identified as cinnamic acid according to the ion fragment.

TABLE 1: Summary of the photolysis products of cinnamyl alcohol by gas chromatography–mass spectrometry and liquid chromatography–quadrupole-time-of-flight–mass spectrometry

Name (abbreviation)	*m/z*	Formula	Retention time (min)	Structure
Cinnamyl alcohol	134.18	$C_9H_{10}O$	9.9[a]	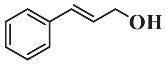
Benzenepropanal	134.18	$C_9H_{10}O$	9.3[a]	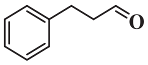
Cinnamyl aldehyde	132.16	C_9H_8O	8.7[a]	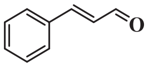
Benzaldehyde	106.12	C_7H_6O	7.8[a]	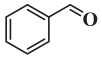
Toluene	92.14	C_7H_8	7.6[a]	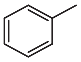
Cinnamic acid	148.16	$C_9H_8O_2$	1.8[b]	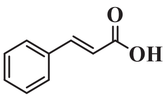

---

[a] Gas chromatography–mass spectrometry retention time.
[b] Liquid chromatography–quadrupole-time-of-flight–mass spectrometry retention time.

The possible chemical structure was assessed for each peak (Table 1). After 90 min of UV light exposure and with the calculation on the basis of GC-MS total ion chromatogram peak areas, the almost total loss of CAL could be explained by the presence of the observed products. These results indicated that the primary photodegradation products of CAL could be degraded into other intermediates as well.

Evaluation of the toxicity of CAL and its degradation products

Generally, the manufacturers and distributors would address the issue of fragrance ingredient safety in their newly developed products; however, there are still many blind spots in these studies. As reported, fragrance ingredients such as acetylethyltetramethyltetralin, musk ambrette, and musk xylol can trigger disorders of the central nervous system, asthma, allergic or nonallergic rhinitis, or chronic respiratory disease (Zhang et al. 2013; Pablos et al. 2015). Therefore, the present study evaluated toxicity and irritation at different stages of the CAL photodegradation process.

By comparing the inhibition of bioluminescence for the phototransformed intermediates of CAL to that of the standards, it was seen that the phototransformation products possessed higher toxicity than the parent compound (Supplemental Data, Figure S6). The initial lethality of the bioluminescence bacteria was 10.63% for the CAL solution, indicating that it has a certain level of biological toxicity. However, the toxicity of the photogenerated products demonstrated 50.19% inhibition after 90-min UV irradiation, indicating that their harmful effect toward *P. phosphoreum* was much higher than that of the parent compound. These toxicity assessments confirmed that more toxic intermediates were produced during photoirradiation; this is a serious concern from an environmental viewpoint because UV light illumination is an important technology for water disinfection in wastewater treatment.

In view of the acute toxicity analysis, it can be concluded that CAL has toxic effects toward aquatic organisms. To further analyze whether or not it has an effect on human health, the irritation risks of CAL and its photodegradation products were assessed theoretically using ACD/Percepta. Irritation analysis was based on the possible cause of the increased stimulus for the eyes and skin of the model animal rabbit (Cunha et al. 2016; Alves et al. 2018); the higher the probability, the more likely the compound is to produce moderate or higher stimuli (Alves et al. 2018). Calculation results are shown in Figure 2. It was found that the probability of skin irritation from the photodegradation products (cinnamic acid [0.83], benzenepropanal [0.69], cinnamyl aldehyde [0.69], and benzaldehyde [0.70]) was higher than that of CAL (0.63). However, as for the probability of eye irritation, only cinnamic acid (0.94) was higher than the probability found for CAL (0.91), though all had the potential to cause eye irritation. Nonetheless, it can be concluded that all the products had a certain irritation effect to the skin and eyes, and some are more likely to cause allergies than the parent compound, making the degraded aqueous solution more allergenic. These allergic contact dermatitis reactions can dramatically impact quality of life as well as the working ability of individuals and are prevalent occupational and environmental diseases (Alves et al. 2016). Therefore, in the future, further environmental investigations and analyses of the ecological toxicity of alcohol fragrances should be taken into consideration for not only the original compounds but also their phototransformation by-products, intermediates, or end products.

Identification of reactive species and transient intermediates

The photodegradation behavior of CAL under UV irradiation was investigated to reveal its fate in water, and the reactive species and transient intermediates were verified. This information will help in understanding the degradation mechanism of CAL and the relationship between toxicity and degradation.

Firstly, the presence of hydroxyl radicals ($^{\bullet}OH$), singlet oxygen ($^1O_2$), and superoxide radicals ($O_2^{\bullet-}$) in the CAL aqueous solutions was detected during the UV irradiation process using EPR spectra. After addition of CAL, as shown in Figure 3A, the peak intensities of DMPO-$O_2^{\bullet-}$ were significantly induced as illumination time increased; this is seen through the 6 typical characteristic peaks of DMPO-$O_2^{\bullet-}$ spin adducts ($a_N = 14$ G, $a_H = 8$ G) in methanol solution as found in previously published reports (Villamena et al. 2005; Tiwari et al. 2013; Ragul et al. 2020). These spin-trap experiments demonstrated that $O_2^{\bullet-}$ radicals played a role in the transformation of CAL under UV light irradiation. Furthermore, TEMP was added to the CAL solution to present proof for $^1O_2$ participation in the reaction (Nardi et al. 2014; Qu et al. 2018). As Figure 3B demonstrates, the EPR spectrum possessed a triplet of lines, with parameters of hyperfine constant aN = 1.63 mT and g value = 2.000. The spectrum intensity increased with prolonged lighting time. These parameters were in good agreement with those of commercial TEMP-O radicals from the

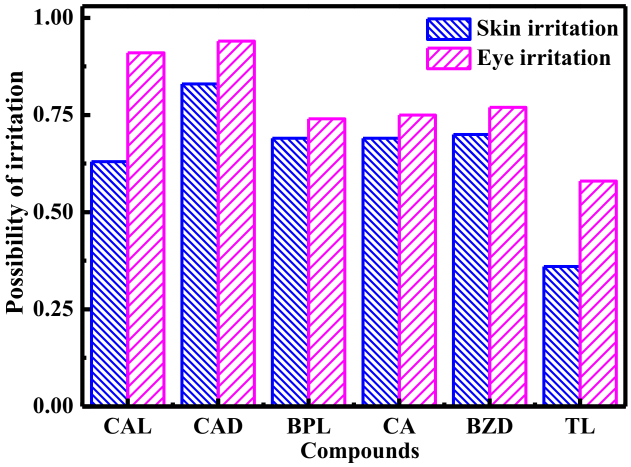

FIGURE 2: The skin and eye irritation analysis of cinnamyl alcohol and its by-products. CAL = cinnamyl alcohol; CAD = cinnamyl aldehyde; BPL = benzenepropanal; CA = cinnamic acid; BZD = benzaldehyde; TL = toluene.

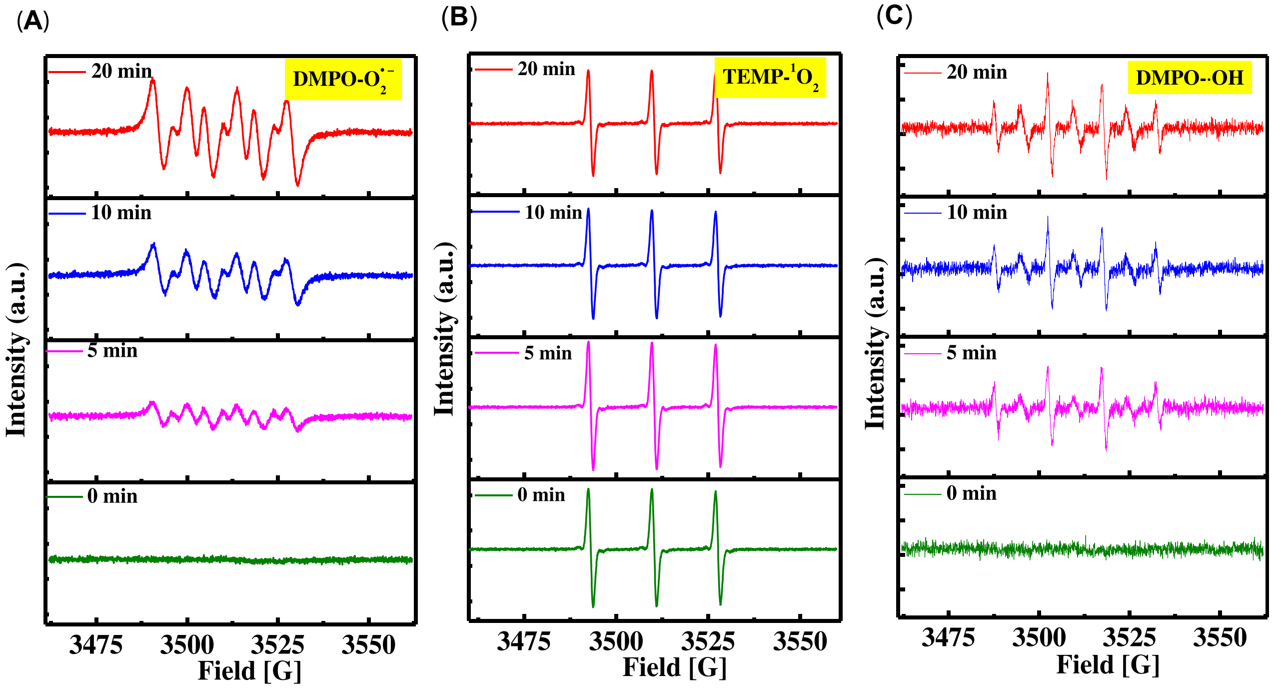

FIGURE 3: The analysis of the active species ($O_2^{\bullet-}$, $^1O_2$, •OH) in the cinnamyl alcohol aqueous solution by electron paramagnetic resonance. DMPO = dimethyl pyridine *N*-oxide; TEMP = 2,2,6,6-tetramethylpiperidine; a.u. = arbitrary units.

reaction of $^1O_2$ with TEMP (Zang et al. 1995). Regarding the formation of $^1O_2$, natural sensitizers might serve as the photosensitizers under aerobic conditions, which then might convert an oxygen molecule to $^1O_2$ (Yang et al. 2020); this can then react with the organic compound CAL. In addition, the typical DMPO-OH adduct can be formed by the reaction of DMPO with •OH (Han et al. 2011; Qu et al. 2018), which can confirm the generation of •OH during the photodegradation of CAL. The spectrum of DMPO-OH exactly matched with the previous parameters, as presented in Figure 3C, which is composed of a quartet of lines with a peak height ratio of 1:2:2:1 and the hyperfine constants ($a_N = a_H = 1.5$ mT and g value = 2.000). Based on the results of EPR, it can be confirmed that $O_2^{\bullet-}$, $^1O_2$, and •OH were involved in the photoreaction with CAL under UV light irradiation.

To explore the evolution of the transient intermediates during the UV photolysis of CAL, LFP experiments with 50 µM CAL were further performed. Figure 4 shows strong absorption peaks at 320 nm and a wide band from 500 to 800 nm, which may be the excited triplet and hydrated electrons (Yuan et al. 2012; An et al. 2014; Fang et al. 2017). As shown in Figure 5, transient species with maximum absorption at 320 nm swiftly increased in saturation of N_2 and decreased in the presence of O_2, which can be expected in that N_2 and O_2 are the protector and scavenger of the excited state, respectively. The transient species with an absorption band ranging from 500 to 800 nm was also able to be quenched by O_2 because of the e_{aq}^- (hydrated electron; Yuan et al. 2012; Radomska et al. 2018). In addition, an LFP experiment of the CAL solution containing 20% MeCN was conducted to further determine the properties of the compounds for the 500- to 800-nm absorption peaks because e_{aq}^- can be quenched by MeCN (Singh et al. 1968; Zhang et al. 2012). Thus, the characteristic transient absorption peaks at 320 and 500 to 800 nm could be identified as the excited state of CAL ($^3CAL^*$) and e_{aq}^-, respectively. The mechanism in 266-nm LFP of CAL solution is demonstrated as in Equations 1 and 2.

$$\mathrm{CAL} \xrightarrow{hv} {}^1\mathrm{CAL}^* \xrightarrow{isc} {}^3\mathrm{CAL}^* \tag{1}$$

$$\mathrm{CAL} \xrightarrow{hv} \mathrm{CAL}^{+} + e_{aq}^- \tag{2}$$

Further, the respective contribution rate was obtained to analyze the role of the main active species during

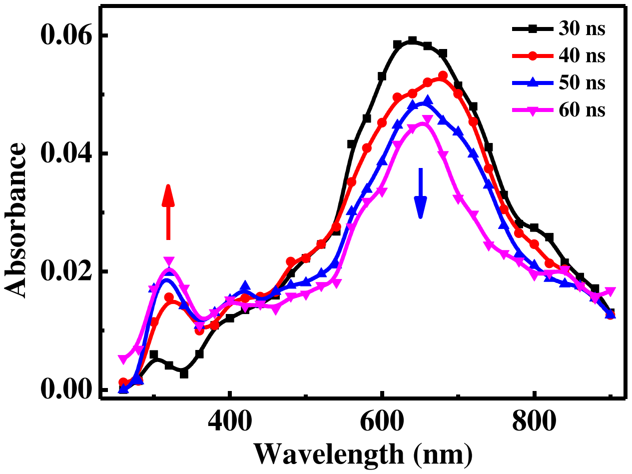

FIGURE 4: The transient absorption spectra at different time intervals of 50 µM cinnamyl alcohol in pure water.

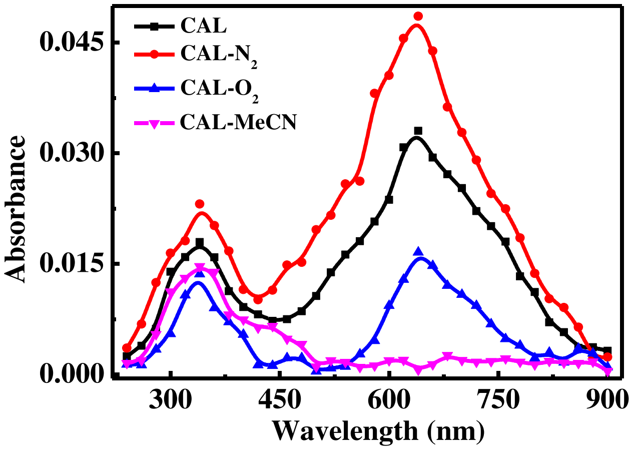

FIGURE 5: Transient absorption spectra of 50 μM cinnamyl alcohol in air, N_2-, and O_2-saturated solution with a ventilation flow rate of 0.1 m s^{-1} and quenching agent (20% MeCN solution) at 150 ns. CAL = cinnamyl alcohol; MeCN = acetonitrile (methyl cyanide).

photodegradation. Special experiments with various scavengers, including p-BQ, FFA, isopropanol, triethanolamine, MeCN, acetone, and different gas saturation (air and N_2), were designed to identify the main reactive species generated during the photodegradation of CAL (An et al. 2014). As shown in Figure 6, the degradation rate of CAL was accelerated under nitrogen and acetone but slowed down under other quenching conditions. In addition, the observed pseudo-first-order degradation rate constants were obtained from degradation curves (Supplemental Data, Table S2). An obvious suppression of CAL photodegradation was seen in the presence of p-BQ, which is a well-known scavenger of superoxide radicals (Xing et al. 2013); this indicated that $O_2^{\bullet-}$ was tremendously contributive to the CAL photodegradation (42.0% contribution). Similarly, the result from quenching with FFA confirmed that $^1O_2$ contributed to approximately 34.2% of CAL photodegradation. When $^\bullet$OH was quenched by isopropanol, photodegradation of CAL was slightly inhibited (~14.3%), indicating that $^\bullet$OH was involved in the reaction but did not contribute much. In addition, the reaction rate constants with and without the protection or stimulation of the excited state of CAL (^{3}CAL*) were measured using N_2 or acetone, respectively. The degradation rate of CAL under nitrogen or acetone was faster, with degradation half-lives of 5.01 and 2.52 min, suggesting that ^{3}CAL* contributed during this photodegradation process (Supplemental Data, Table S2). Furthermore, when ^{3}CAL* was quenched by triethanolamine, the photodegradation rate of CAL decreased to 91.2%, indicating that ^{3}CAL* does participate in the reaction. These results are in good agreement with data showing that some reactive intermediates such as bromophenols (Bertoti et al. 2015; Jiang et al. 2017; Fujitsuka and Majima 2018) could be produced in this process (with a contribution of 8.7%). In addition, low inhibition (0.4%) of CAL photodegradation was observed when the e_{aq}^- was excluded by addition of the quencher MeCN. From these results, it can be concluded that $O_2^{\bullet-}$, $^1O_2$, and $^\bullet$OH were the main reactive species during photodegradation and were largely responsible for the photodegradation of CAL (contribution rates of 42.0, 34.2, and 14.3%, respectively). Along with these, ^{3}CAL* and e_{aq}^- also participate in this reaction.

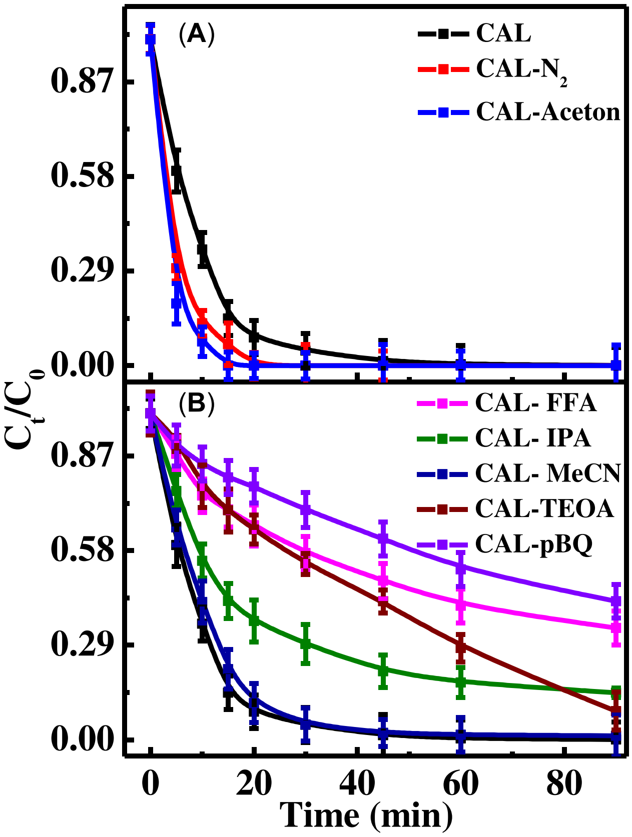

FIGURE 6: Degradation kinetics of 50 μM cinnamyl alcohol under UV irradiation with (**A**) no scavenger, N_2-saturated solution, or 10% acetone solution, and (**B**) quenching agents (100 μM furfuryl alcohol, 5 mM isopropanol, in 20% acetonitrile solution, 5 mM triethanolamine, and 5 mM p-benzoquinone). CAL = cinnamyl alcohol; FFA = furfuryl alcohol; IPA = isopropanol; MeCN = acetonitrile (methyl cyanide); TEOA = triethanolamine; pBQ = p-benzoquinone.

The photochemical degradation mechanism

The photodegradation product was not observed by MS; either it degraded faster than it was formed or it was too difficult to analyze using LC-Q-TOF/MS and GC-MS. Based on the results from the identification of intermediates and the confirmation of reactive species, schematic reaction pathways for the photodegradation of CAL were suggested. As shown in Figure 7, photochemical degradation mechanisms of CAL mostly involved $O_2^{\bullet-}$ or $^1O_2$–, $^\bullet$OH–, ^{3}CAL*-, and e_{aq}^--mediated reaction pathways.

$O_2^{\bullet-}$- or $^1O_2$-mediated reaction pathways. $O_2^{\bullet-}$ is generated through a reaction of molecular oxygen, which leads to the oxidation of double bonds of the organics (Sugimoto et al. 1987). In the present study, CAL could be easily oxidized to cinnamyl aldehyde and then to cinnamic acid once exposed to the air (Niklasson et al. 2013), which may be a main pathway leading to toxicity enhancement.

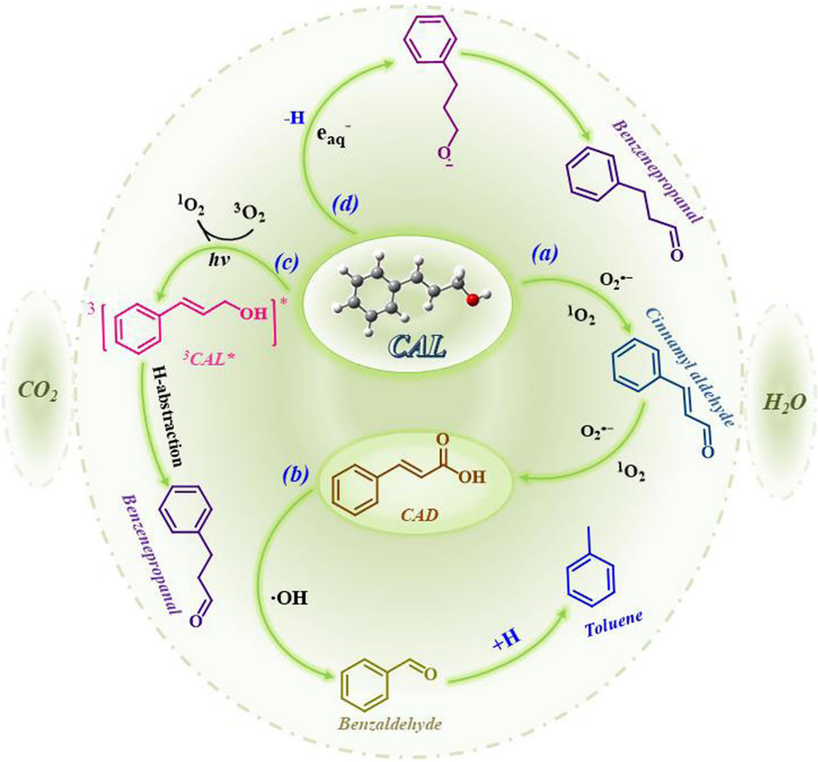

FIGURE 7: The photochemical degradation pathways of cinnamyl alcohol. CAL = cinnamyl alcohol; CAD = cinnamyl aldehyde.

•OH-mediated reaction pathways. Hydroxylation at the other side of the double bond of cinnamic acid, followed by attaching the superoxide or oxygen at the radical center and a reverse-aldol reaction cleaving the C–C bond, produces benzaldehyde as well as O=CH–CO_2H; this has been documented as an important pathway for the reaction of •OH with cinnamic acid (Santos and Vieira 2013). Benzaldehyde is a reactive chemical (Jin et al. 1998), which exhibits bioreactive toxicity to increase the overall toxicity of the system. The subsequent steps in the photodegradation reaction may be involved in the attack of +H on –CHO, resulting in toluene intermediates through a reduction reaction because toluene can produce benzaldehyde under the action of a hydroxyl group oxidation reaction which tends to undergo a substitution reaction or hydrogen abstraction (Homlok et al. 2020; Salta et al. 2020).

^{3}CAL*-mediated reaction pathways. The excited state of CAL, ^{3}CAL*, can be generated from CAL by absorption of photon energy, following which $^1O_2$ could have be produced when the excited singlet and triplet states were quenched by the ground state molecular oxygen. In this photolysis process benzenepropanal was the most likely by-product to be produced.

e_{aq}^--mediated reaction pathways. Possibly, CAL could be attacked by e_{aq}^- generated during this process, leading to the formation of the dehydrogenation intermediate benzenepropanal.

To further identify the mineralization of these intermediates, the TOC contents of the CAL reaction as a function of photolysis time were determined (Supplemental Data, Figure S7). Although the concentration of CAL decreased dramatically during the first 15 min of the reaction, the TOC content did not drop significantly, only decreasing by 0.31 mg L^{-1}. Over the total irradiation time (90 min), TOC only decreased from 5.89 to 4.00 mg L^{-1}. This indicated that under the specific irradiation conditions CAL may be mainly transformed into some persistent organic intermediates and not totally mineralized, which needs more study to clarify.

Overall, it can be concluded that during the photochemical degradation of CAL some sensitization, persistence, and bioaccumulating intermediates might be produced, possibly resulting in adverse effects on environmental and human health. Thus, the ecotoxicity of these photodegradation intermediates as well as the parent compound CAL should not be neglected.

CONCLUSIONS

In the present study, the phototransformation mechanisms of CAL under UV light irradiation were investigated. The persistent intermediates were identified, and their chemical structures were confirmed by MS analysis. During the photochemical degradation process, cinnamyl aldehyde, cinnamic acid, benzaldehyde, toluene, and benzenepropanal were initially generated from $O_2^{\bullet-}$ or $^1O_2$–, •OH–, ^{3}CAL*–, and e_{aq}^--mediated reactions. The main active species, $O_2^{\bullet-}$, $^1O_2$, and •OH, were found in photodegradation quenching experiments. The EPR spectra of aqueous CAL helped to confirm that $^1O_2$, $O_2^{\bullet-}$, and •OH were present during photoirradiation. In addition, the transient intermediates were identified with LFP using a 266-nm laser pulse and could be photolyzed to generate ^{3}CAL* and e_{aq}^- at 320 and 640 nm, respectively. Finally, the irritation prediction and preliminary toxicity investigations provided evidence that more toxic compounds were produced during the photo-irradiation procedure. The knowledge gained in the present study should help in developing guidance for the assessment of aquatic environmental fates of other fragrance chemicals.

Supplemental Data—The Supplemental Data are available on the Wiley Online Library at https://doi.org/10.1002/etc.5156.

Acknowledgment—The present study was supported by the National Natural Science Foundation of China (41425015, 41977365, and 21607028), the Local Innovative and Research Teams Project of the Guangdong Pearl River Talents Program (2017BT01Z032), and the Science and Technology Program of Guangzhou, China (201804010128).

Disclaimer—The authors declare no competing interest.

Author Contributions Statement—J. Wu was responsible for formal analysis, investigation, methodology, validation, and writing the original draft; Y. Gao was responsible for review of writing and editing and validation; T. Guo was responsible for data curation; N. Luo commented on previous versions of the manuscript; G. Li was responsible for review of writing and editing; T. An was responsible for conceptualization, validation, review of writing and editing, supervision, and funding acquisition. All authors read and approved the final manuscript.

Data Availability Statement—Data, associated metadata, and calculation tools are available from the corresponding author (antc99@gdut.edu.cn).

REFERENCES

Alves VM, Capuzzi SJ, Braga RC, Borba JVB, Silva AC, Luechtefeld T, Hartung T, Andrade CH, Muratov EN, Tropsha A. 2018. A perspective and a new integrated computational strategy for skin sensitization assessment. *ACS Sustain Chem Eng* 6(3):2845–2859.

Alves VM, Capuzzi SJ, Muratov EN, Braga RC, Thornton TE, Fourches D, Strickland J, Kleinstreuer N, Andrade CH, Tropsha A. 2016. QSAR models of human data can enrich or replace LLNA testing for human skin sensitization. *Green Chem* 18:6501–6515.

An TC, Fang HS, Li GY, Wang SL, Yao SD. 2014. Experimental and theoretical insights into photochemical transformation kinetics and mechanisms of aqueous propylparaben and risk assessment of its degradation products. *Environ Toxicol Chem* 33:1809–1816.

Banihani Q, Sierra-Alvarez R, Field JA. 2009. Nitrate and nitrite inhibition of methanogenesis during denitrification in granular biofilms and digested domestic sludges. *Biodegradation* 20:801–812.

Basketter DA. 1992. Skin sensitization to cinnamic alcohol: The role of skin metabolism. *Acta Derm Venereol* 72:264–265.

Bertoti AR, Guimaraes AK, Netto-Ferreira JC. 2015. Laser flash photolysis study of the photochemistry of 4,5-diaza-9-fluorenone. *J Photochem Photobiol A Chem* 299(15):166–171.

Bickers D, Calow P, Greim H, Hanifin JM, Rogers AE, Saurat JH, Sipes IG, Smith RL, Tagami H. 2005. A toxicologic and dermatologic assessment of cinnamyl alcohol, cinnamaldehyde and cinnamic acid when used as fragrance ingredients. *Food Chem Toxicol* 43:799–836.

Bridges B. 1999. Fragrances and health. *Environ Health Perspect* 107:A340.

Chen G, Liu F, Qiao Y, Tao B. 2019. Photodegradation of tefuryltrione in water under UV irradiation: Identification of transformation products and elucidation of photodegradation pathway. *Chemosphere* 227:133–141.

Cheung C, Hotchkiss SAM, Pease CKS. 2003. Cinnamic compound metabolism in human skin and the role metabolism may play in determining relative sensitisation potency. *J Dermatol Sci* 31:9–19.

Cunha M, Franco G, Franchin M, Beutler JA, Alencar SD, Ikegaki M, Rosalen PL. 2016. Prediction of pharmacokinetic and toxicological parameters of a 4-phenylcoumarin isolated from geopropolis: In silico and in vitro approaches. *Toxicol Lett* 263:6–10.

Fang H, Gao Y, Li G, An J, Wong P-K, Fu H, Yao S, Nie X, An T. 2013. Advanced oxidation kinetics and mechanism of preservative propylparaben degradation in aqueous suspension of TiO_2 and risk assessment of its degradation products. *Environ Sci Technol* 47:2704–2712.

Fang H, Gao Y, Wang H, Yin H, Li G, An T. 2017. Photo-induced oxidative damage to dissolved free amino acids by the photosensitizer polycyclic musk tonalide: Transformation kinetics and mechanisms. *Water Res* 115:339–346.

Fujitsuka M, Majima T. 2018. Reaction dynamics of excited radical ions revealed by femtosecond laser flash photolysis. *J Photochem Photobiol C Photochem Rev* 35:25–37.

Godayol A, Gonzalez-Olmos R, Sanchez JM, Antico E. 2015. Assessment of the effect of UV and chlorination in the transformation of fragrances in aqueous samples. *Chemosphere* 125:25–32.

Han SK, Hwang T-M, Yoon Y, Kang J-W. 2011. Evidence of singlet oxygen and hydroxyl radical formation in aqueous goethite suspension using spin-trapping electron paramagnetic resonance (EPR). *Chemosphere* 84:1095–1101.

Homlok R, Mile V, Takács E, Járvás G, Wojnárovits L. 2020. Comparison of hydrogen atom and hydroxyl radical reactions with simple aromatic molecules in aqueous solution. *Chem Phys* 534:110754.

Janzen N, Dopp E, Hesse J, Richards J, Tuerk J, Bester K. 2011. Transformation products and reaction kinetics of fragrances in advanced wastewater treatment with ozone. *Chemosphere* 85:1481–1486.

Jiang J, Zhao H, Liu S, Chen X, Jiang X, Chen J, Quan X. 2017. Photochemical reactions between bromophenols and hydroxyl radical generated in aqueous solution: A laser flash photolysis study. *J Photochem Photobiol A Chem* 336:63–68.

Jin L, Dai J, Guo P, Wang L, Wei Z, Zhang Z. 1998. Quantitative structure–toxicity relationships for benzaldehydes to *Daphnia magna*. *Chemosphere* 37:79–85.

Johansen JD, Rastogi SC, Menne T. 1996. Exposure to selected fragrance materials. A case study of fragrance-mix-positive eczema patients. *Contact Dermatitis* 34:106–110.

Katsarou A, Armenaka M, Kalogeromitros D, Koufou V, Georgala S. 1999. Contact reactions to fragrances. *Ann Allergy Asthma Immunol* 82:449–455.

Letizia CS, Cocchiara J, Lalko J, Lapczynski A, Api AM. 2005. Fragrance material review on cinnamyl alcohol. *Food Chem Toxicol* 43:837–866.

Lopez SH, Hernando MD, Gomez MJ, Santiago-Morales J, Rosal R, Fernandez-Alba AR. 2013. Investigation of galaxolide degradation products generated under oxidative and irradiation processes by liquid chromatography/hybrid quadrupole time-of-flight mass spectrometry and comprehensive two-dimensional gas chromatography/time-of-flight mass spectrometry. *Rapid Commun Mass Spectrom* 27:1237–1250.

Nardi G, Manet I, Monti S, Miranda MA, Lhiaubet-Vallet V. 2014. Scope and limitations of the TEMPO/EPR method for singlet oxygen detection: The misleading role of electron transfer. *Free Radic Biol Med* 77:64–70.

Niklasson IB, Delaine T, Islam MN, Karlsson R, Luthman K, Karlberg A-T. 2013. Cinnamyl alcohol oxidizes rapidly upon air exposure. *Contact Dermatitis* 68:129–138.

Pablos MV, García-Hortigüela P, Fernández C. 2015. Acute and chronic toxicity of emerging contaminants, alone or in combination, in *Chlorella vulgaris* and *Daphnia magna*. *Environ Sci Pollut Res* 22:5417–5424.

Peng X, Zhu Z, Xiong S, Fan Y, Chen G, Tang C. 2020. Tissue distribution, growth dilution, and species-specific bioaccumulation of organic ultraviolet absorbents in wildlife freshwater fish in the Pearl River catchment, China. *Environ Toxicol Chem* 39:343–351.

Pinkas A, Goncalves CL, Aschner M. 2017. Neurotoxicity of fragrance compounds: A review. *Environ Res* 158:342–349.

Qu R, Li C, Liu J, Xiao R, Pan X, Zeng X, Wang Z, Wu J. 2018. Hydroxyl radical based photocatalytic degradation of halogenated organic contaminants and paraffin on silica gel. *Environ Sci Technol* 52: 7220–7229.

Radomska K, Konarska A, Wolszczak M. 2018. Scavenging of hydrated electron by HSA or ligand/HSA adduct: Pulse radiolysis study. *Radiat Phys Chem* 152:23–35.

Ragul K, Kandasamy S, Devi PB, Shetty PH. 2020. Evaluation of functional properties of potential probiotic isolates from fermented brine pickle. *Food Chem* 311:126057.

Research Institute for Fragrance Materials. 1987. The dermal absorption of 14C-2-phenylethanol in man following a single topical application. Report 14275. Woodcliff Lake, NJ, USA.

Riyad YM. 2017. Thioanisole triplet: Laser flash photolysis and pulse radiolysis studies. *J Photochem Photobiol A Chem* 335:294–299.

Salta Z, Kosmas AM, Segovia ME, Kieninger M, Tasinato N, Barone V, Ventura ON. 2020. Reinvestigation of the deceptively simple reaction of toluene with OH and the fate of the benzyl radical: The "hidden" routes to cresols and benzaldehyde. *J Phys Chem A* 124: 5917–5930.

Santos PMP, Vieira AJSC. 2013. Antioxidising activity of cinnamic acid derivatives against oxidative stress induced by oxidising radicals. *J Phys Org Chem* 26:432–439.

Sealey LA, Hughes BW, Steinemann A, Pestaner JP, Pace DG, Bagasra O. 2015. Environmental factors may contribute to autism development and male bias: Effects of fragrances on developing neurons. *Environ Res* 142:731–738.

Singh A, Gesser HD, Scott AR. 1968. Solvated electron in acetonitrile. *Chem Phys Lett* 2:271–273.

Smith CK, Moore CA, Elahi EN, Smart AT, Hotchkiss SA. 2000. Human skin absorption and metabolism of the contact allergens, cinnamic aldehyde, and cinnamic alcohol. *Toxicol Appl Pharmacol* 168:189–199.

Sugimoto H, Matsumoto S, Sawyer DT. 1987. Oxygenation of polychloro aromatic hydrocarbons by superoxide ion in aprotic media. *J Am Chem Soc* 109:8081–8082.

Thyssen JP, Johansen JD, Linneberg A, Menné T. 2010. The epidemiology of hand eczema in the general population—Prevalence and main findings. *Contact Dermatitis* 57:287–299.

Tiwari A, Rac M, Pospisil P. 2013. Formation of superoxide anion and carbon-centered radicals by photosystem II under high light and heat stress-EPR spin-trapping study. *J Bioenerg Biomembr* 45:551–559.

Uter W, Hegewald J, Aberer W, Ayala F, Bircher AJ, Brasch J, Coenraads PJ, Schuttelaar ML, Elsner P, Fartasch M. 2010. The European standard series in 9 European countries, 2002/2003—First results of the European Surveillance System on Contact Allergies. *Contact Dermatitis* 61:31–38.

Villamena FA, Merle JK, Hadad CM, Zweier JL. 2005. Superoxide radical anion adduct of 5,5-dimethyl-1-pyrroline *N*-oxide (DMPO). 1. The thermodynamics of formation and its acidity. *J Phys Chem A* 109: 6083–6088.

Wu J, Gao Y, Qin Y, Li G, An T. 2021. Photochemical degradation of fragrance ingredient benzyl formate in water: Mechanism and toxicity assessment. *Ecotoxicol Environ Saf* 211:111950.

Xing R, Wu L, Fei Z, Wu P. 2013. Mesopolymer modified with palladium phthalocyaninesulfonate as a versatile photocatalyst for phenol and bisphenol A degradation under visible light irradiation. *J Environ Sci* 25:1687–1695.

Yang J, Zhu W, Yao Q, Lu G, Yang C, Dang Z. 2020. Photochemical reactivity of nitrogen-doped biochars under simulated sunlight irradiation: Generation of singlet oxygen. *J Hazard Mater* 410:124547.

Yuan HX, Pan HX, Yan-Lin WU, Zhao JF, Dong WB. 2012. Laser flash photolysis mechanism of pyrenetetrasulfonate in aqueous solution. *Acta Physico-Chimica Sinica* 28:957–962.

Zang LY, van Kuijk FJ, Misra BR, Misra HP. 1995. The specificity and product of quenching singlet oxygen by 2,2,6,6-tetramethylpiperidine. *Biochem Mol Biol Int* 37:283–293.

Zhang B, Li K, Cao C, Wang M, Chen Q, Wang S. 2012. The laser flash photolysis and UV photolytical degradation of 4-n-nonylphenol. *Sci Sin* 42:175–181.

Zhang W, Gao Y, Qin Y, Wang M, Wu J, Li G, An T. 2019. Photochemical degradation kinetics and mechanism of short-chain chlorinated paraffins in aqueous solution: A case of 1-chlorodecane. *Environ Pollut* 247: 362–370.

Zhang XL, Brar SK, Yan S, Tyagi RD, Surampalli RY. 2013. Fate and transport of fragrance materials in principal environmental sinks. *Chemosphere* 93:857–869.